OPEN ACCESS
ACTA METALLURGICA SLOVACA
2025, VOL. 31, NO. 4, 212-218

The influence of heat input in orbital TIG welding on various diameters and thicknesses of low-carbon steel tube

Ngoc-Thien Tran[1,2], Van-Sung Nguyen[1], Van-Thuc Nguyen[1,], Nguyen Cong Thinh[1], Nguyen Trung Quoc Ngoc[1], Ho Cong Tung[1]*

1 HCMC University of Technology and Education, Ho Chi Minh City, Vietnam
2 PhD student, HCMC University of Technology and Education, Ho Chi Minh City, Vietnam

*Corresponding author: nvthuc@hcmute.edu.vn, tel.: [+84]949718680, HCMC University of Technology and Education, 71307, Ho Chi Minh City, Vietnam

Received: 20.08.2025
Accepted: 09.09.2025

ABSTRACT

Partial joint penetration (PJP) welding is widely applied in structural, mechanical, and piping systems where full penetration is not required, offering benefits in cost, time efficiency, and reduced heat input. The main goal was to evaluate the effects of Heat Input on the weld geometry and ultimate tensile strength of low-carbon steel tubes. Therefore, the welds were carried out using Orbital TIG Welding, designed to achieve partial joint penetration (PJP). The number of experiments and the welding parameter matrix were created using the Taguchi method (L9) for various diameters of Ø48×3.2mm, Ø60×2.6mm, and Ø89×2.9mm. The results indicated that, under the same Heat Input levels, variations in tube thickness had a greater impact on weld profile and ultimate tensile strength than changes in diameter. Furthermore, the ANOVA analysis ranks the influence of welding factors on tensile strength. This study proposes an optimal set of welding parameters and predicts the corresponding tensile strength for each pipe diameter, thereby providing valuable insights for improving the reliability and performance of welded joints.

Keywords: Low-carbon tubes; OTW parameters; Heat Input; PJP.

INTRODUCTION

Low–carbon steel pipes play a fundamental role in modern industrial applications due to their excellent mechanical properties, affordability, and ease of fabrication. Defined by carbon content typically below 0.3%, low carbon steel (also referred to as mild steel) offers a balance between strength, ductility, and weldability, making it one of the most widely used materials across various sectors, including construction, oil and gas, water treatment, automotive, manufacturing, and power generation [1]. The widespread use of low-carbon steel pipes is largely attributed to their economic efficiency and material performance. Compared to higher alloy steels or non-ferrous metals, low-carbon steel is significantly more cost-effective, making it an ideal material for large-scale infrastructure projects and industrial networks [2]. Additionally, its formability and machinability enable efficient manufacturing processes, including cutting, bending, and welding. From a mechanical standpoint, low-carbon steel pipes provide sufficient tensile strength and toughness for a wide range of structural and fluid transport applications. While not as hard or resistant as high carbon steels, their high ductility allows for deformation without fracture, which is especially advantageous in dynamic or seismic environments [3].

In pipeline systems, the ability to absorb energy and resist crack propagation is vital, especially in applications involving vibration or variable pressure. However, Heat Input (HI) has a significant influence on the mechanical properties and microstructure of both the weld zone and the heat-affected zone (HAZ) in low-carbon steel welds. Bodude et al. [4] investigated the influence of heat input on the mechanical properties of low-carbon steel by employing Oxy-Acetylene Welding and Shielded Metal Arc Welding techniques. It was found that tensile strength and hardness decreased with increased HI, while impact strength increased. Additionally, the result of this research revealed that the chemical composition of steel significantly affects weldability and mechanical properties, with elements such as carbon and Manganese enhancing strength but increasing the risks of cracking and grain coarsening during welding. According to the study of Panji et al. [5], this study investigates the effects of welding current and welding speed on the weld geometry and distortion of A36 mild steel pipes during the TIG welding process with a V-groove joint. The findings indicate that increasing the welding current widens the weld bead and increases distortion levels, while varying the welding speed has a minimal impact on these parameters. Notably, the optimal parameters for achieving the widest outer bead and the highest distortion were established at a welding current of 170 A and a speed of 0.9 mm/s, with distortion being more pronounced in the axial direction than in the transverse direction. Another key advantage is the excellent weldability of low-carbon steel pipes, which allows for seamless integration into complex pipeline networks using welding processes such as Shielded Metal Arc Welding (SMAW), Gas Tungsten Arc Welding (GTAW), or automated techniques like orbital welding. This facilitates the assembly of long, continuous runs of piping with minimal joints, reducing the potential for leakage and maintenance [6].

Nowadays, Orbital TIG Welding (OTW) is widely used in industries to weld pipes for transporting materials such as oil, gas, food, and beverages [7–11]. Notably, this technology has been extensively researched for stainless steel tubes because OTW stands out as a highly accurate and automated process that enables consistent and defect-free joints, particularly in tubular structures. This method involves rotating the welding arc 360 degrees around a stationary workpiece, typically using a tungsten inert gas (TIG) welding process under computer control (**Fig. 1**).

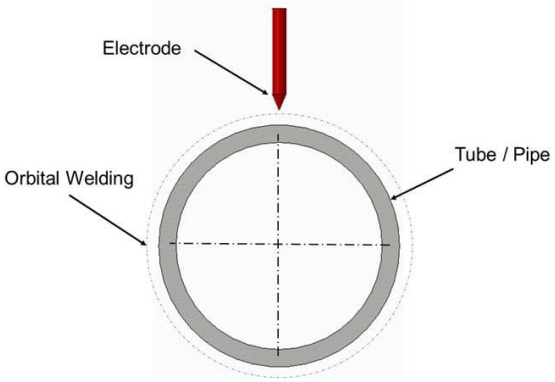

Fig.1 The principle of Orbital TIG welding.

When applied to low-carbon steel, OTW must be carefully optimised to control factors such as thermal conductivity, oxidation, and microstructural changes in the heat-affected zone (HAZ). While low-carbon steels are generally forgiving in terms of weldability, improper heat control or shielding can result in unwanted hardness, grain growth, or residual stresses that affect the mechanical properties of the joint. Therefore, understanding the influence of welding parameters such as current, voltage, arc travel speed, and shielding gas composition on the quality of the weld is essential for ensuring optimal performance. For instance, Hussein et al. [12] investigated the tensile strength of orbital-welded mild steel tubes with dissimilar thicknesses, emphasising the impact of welding current and jig rotational speed on the strength of the welds. It is observed that increasing the welding current enhances tensile strength, whereas higher jig rotational speeds impair it. An empirical mathematical model was developed, demonstrating a high accuracy of 96.8%, which elucidates the relationship between welding

parameters and the ultimate tensile strength. The optimal welding conditions for maximum tensile strength were determined to be 80 A welding current and 40 rpm jig rotational speed when applied to 26.70 mm diameter tubes with varying wall thicknesses. Moreover, Figueirôa et al. [13] investigated the welding efficiency in terms of position and parameters for orbital TIG welding of low-carbon steel pipes. They studied the impact of welding position and parameters on the OTW process of low-carbon steel pipes. It highlights that using pulsed current results in wider and harder weld beads with a finer microstructure, while the vertical up welding position yields better penetration and lower shape factors. Additionally, the research finds that a specific wire speed-to-power ratio is crucial for ensuring stable metal feed during welding, which significantly influences variations in microstructure and hardness. The differences between conditions highlight the effects of heat input, with pulsed current producing smaller prior austenitic grain sizes. According to Ngo et al. [14], automatic welding methods— including continuous, pulsed, and step-pulse modes — each offer unique benefits and applications within welding processes. Furthermore, edge preparation is crucial in welding, as different techniques significantly impact its quality and efficiency. The choice between V-shaped and U-shaped edge cuts is emphasised, as they suit different pipeline wall thicknesses and influence weld quality. An appropriate HI parameter will achieve full penetration welds [15–18]. Excessive heat input can cause the weld to overheat, burn, and distort [5, 15]. Conversely, if the heat input is too low, the weld may not reach sufficient melting and penetration, resulting in poor joints.

Most existing research on low-carbon steel welding has focused on full-penetration welds or butt joints, as they play a critical role in pressure vessels, pipelines, and structural components. Studies have also predominantly focused on the influence of heat input, welding speed, and filler material on the mechanical properties and microstructural evolution in full-penetration welds. In contrast, PJP welds in low-carbon steel tubes have received relatively limited systematic investigation, especially concerning the influence of varying heat input on penetration, microstructure heterogeneity, and residual stress in PJP tube welds, which is not well understood.

MATERIAL AND METHODS

Material

The material used in this paper is low-carbon steel (type F and grade A), complying with ASTM A53/A53M-12 standards [19], with outer diameters of 48mm, 60mm, and 89mm, and respective thicknesses of 3.2mm, 2.6mm, and 2.9mm. The chemical composition and mechanical properties of this basic metal are shown in **Table 1** and **Table 2**.

Table 1 Chemical content of low carbon steel (type F and grade A) [19]

ASTM A53 – Type F	Composition (%), max						
	C	*Mn*	*S*	*P*	*Ni*	*Cr*	*Cu*
Grade A	0.3	1.2	0.0045	0.05	0.4	0.4	0.4

Table 2 Mechanical properties of low carbon steel (type F and grade A) [19]

ASTM A53 – Type F	*Tensile strength, min, MPa*	*Yield strength, min, Mpa*	*Elongation in 50mm, min, %*
Grade A	330	205	36

Methods

The experimental parameter table was established using the Taguchi method, with the three welding parameters —arc current (I), Arc voltage (V), and Welding speed (Vs) — varied at three different levels, as shown in **Table 3**. **Table 3** is the welding parameter table for each diameter. Besides, Heat Input (HI) in welding refers to the total arc energy supplied to the weld pool during the welding process. It's a crucial parameter in arc welding, affecting factors such as weld quality, cooling rates, and the microstructure of the weld and the heat-affected zone (HAZ). Therefore, the HI value is mentioned in this study and calculated according to formula (1.) [20]:

$$HI = \frac{\eta . I . U}{Vs} \quad (1.)$$

Where: HI is heat input (kJ/mm),

I is arc current (A), U is arc voltage (V), and Vs is welding speed (mm/s).

η is the weld thermal efficiency, which is often 0.6 for the GMAW or TIG.

Table 3 *Experimental parameters, HI and Ultimate Tensile Strength*

Code	Welding parameters			Heat Input, HI (j/mm)	Ultimate Tensile Strength, UTS (Mpa)		
	Current, I (A)	*Welding Speed, Vs (mm/s)*	*Voltage, U (V)*		*Ø48*	*Ø60*	*Ø89*
S1	80	144	10	200	124	174	131
S2	80	180	11	180	107	93	67
S3	80	216	13	170	98	66	93
S4	100	144	11	280	109	202	142
S5	100	180	13	260	122	203	76
S6	100	216	10	170	120	48	110
S7	120	144	13	390	241	251	177
S8	120	180	10	240	152	233	133
S9	120	216	11	220	126	188	141

After performing 27 butt welds on pipes of three various diameters, the tensile test locations were selected in accordance with the ASME IX standard and are presented in **Fig. 2a** [21]. The tensile samples are tested according to the ISO 6892-1 standard [22], as shown in **Fig. 2b**.

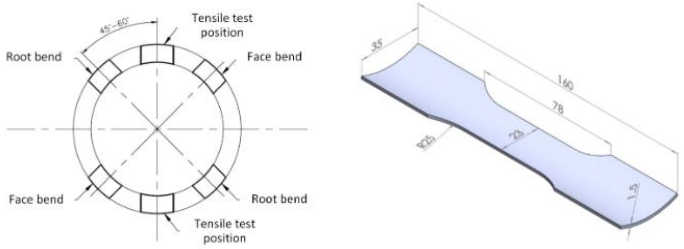

a) Sampling position for tensile test b)Tensile test profile

Fig. 2 Tensile testing sample

To investigate the microstructural changes in welds under the influence of heat input (HI), the specimen preparation process was carried out according to the flowchart shown in the **Fig. 3**. The microstructures of the samples were also observed using an Oxion OX.2153-PLM EUROMEX metallurgical microscope in 6 steps.

Fig. 3 Flow chart of preparation for microstructure sample

RESULTS AND DISCUSSION

Tensile test results

After performing nine welds for each pipe size, the sampling location for UTS testing was selected according to the ASME IX standard (**Fig. 2a**). **Table 3** presents the welding parameters, Heat Input (HI), and Ultimate Tensile Strength (UTS) of the 27 tube welds. The results show that weld S7 had the highest HI value of 390 J/mm, and it also exhibited the highest UTS among the three pipe sizes, Ø48mm, Ø60mm, and Ø89mm, with respective values of 241 MPa, 251 MPa, and 177 MPa. However, these UTS values are still lower than the reference UTS value of 330 MPa listed in **Table 2**. Among the S7 samples, only S7-60 achieved full penetration, while the others exhibited incomplete penetration, as the depth of penetration (DOP) only reached slightly more than half of the pipe wall thickness. This indicates that the HI generated from the selected welding parameters was insufficient to fully melt and fuse the entire cross-section of the joint. In contrast, the S3 and S6 sample groups exhibited the lowest UTS values, as the HI provided for these welds was the lowest, only 170 J/mm. The results of this study once again confirm that HI plays a decisive role in weld quality,

particularly in terms of DOP and UTS [23, 24]. Most of the welds on Ø60mm diameter pipes achieved higher UTS compared to the other two pipe sizes, even at the same HI values. However, samples S3-60 and S6-60 showed the lowest UTS values, at 66 MPa and 48 MPa, respectively, because both samples belonged to the group with the lowest HI. Referring to weld geometries in **Table 4**, welds were created by low HI (under 200J/mm), which were significantly misaligned from the gap.

Table 4 Metallurgraphy of 27 samples on the X100 scale.

Code	Ø48mm	Ø60mm	Ø89mm
S1	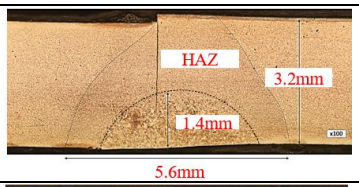	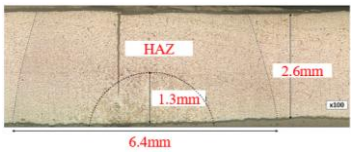	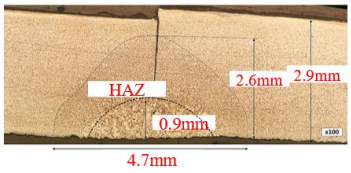
S2	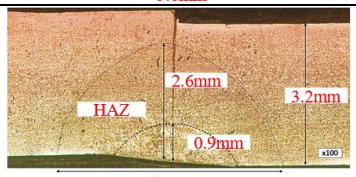	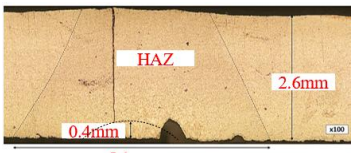	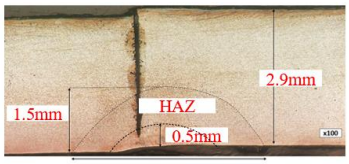
S3	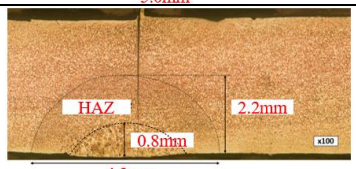	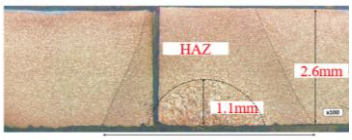	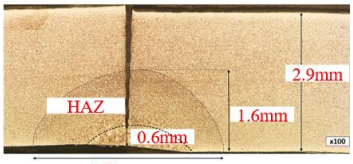
S4	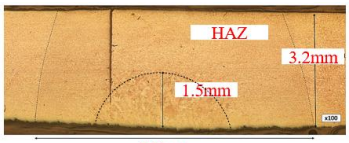	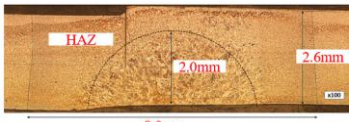	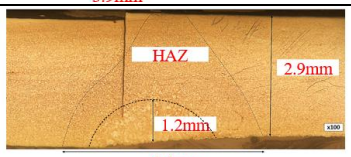
S5	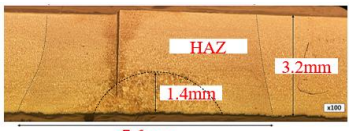	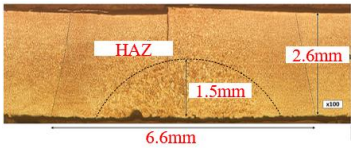	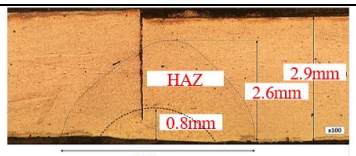
S6	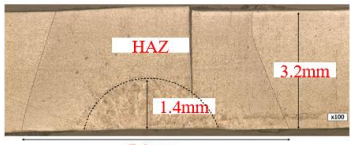	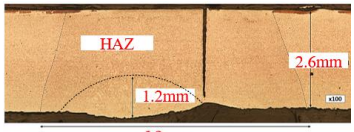	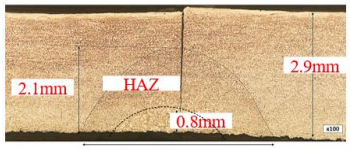
S7	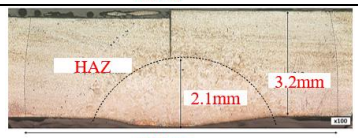		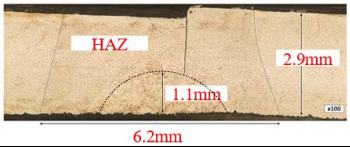
S8	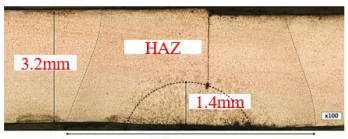	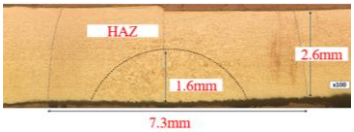	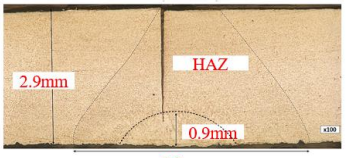
S9	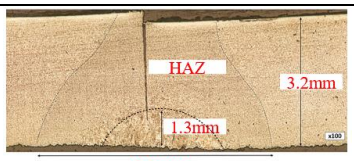	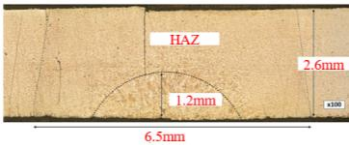	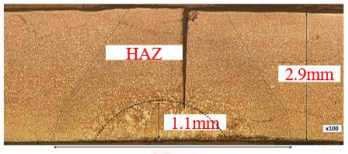

In the case of sample S3-60, the high welding voltage resulting from an excessive arc length could have caused arc deflection during welding. For sample S6-60, the highest welding speed likely led to arc instability throughout the welding process.
In conduction heat transfer [25], the most common means of correlation is through Fourier's Law of Conduction. The law, in its equation form, is used most often in its cylindrical form (pipes and cylinders), which are presented below.

$$\dot{Q} = k.A.\frac{\Delta T}{\Delta r} \quad (2.)$$

Where: $\dot{Q}$ is heat transfer (kW).
A is a cross-sectional area of heat transfer (mm^2).
ΔT is the temperature difference (°F).
Δr is the radius of the cylinder (mm).
k is the coefficient of thermal conductivity of the substance.

From Equation (2.), we can explain the reason why, despite having the same HI levels, the tensile test samples of the Ø60mm pipes (except for samples S2-60, S3-60, and S6-60) generally achieved the highest UTS compared to other diameters. This equation indicates that the rate of heat transfer in the radial direction (**Fig. 5**) depends on the wall thickness (Δr). Therefore, since the Ø60mm pipe has the smallest thickness of 2.6mm, heat is transmitted more quickly through the wall, making the fusion process more efficient and resulting in deeper weld penetration.

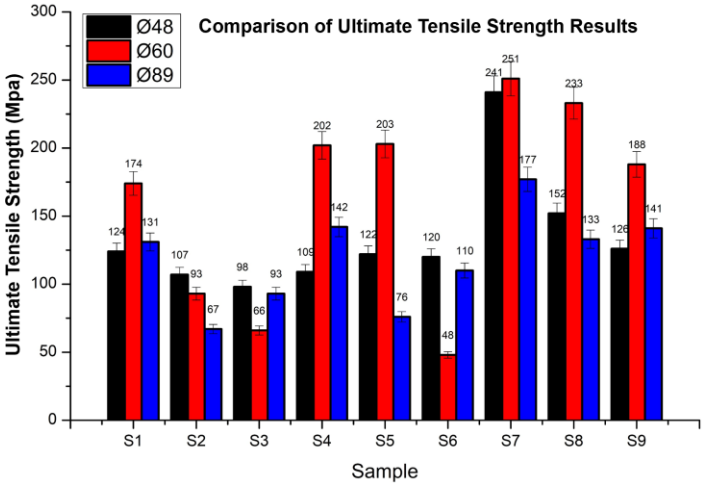

Fig. 4 The chart of comparison of UTS results

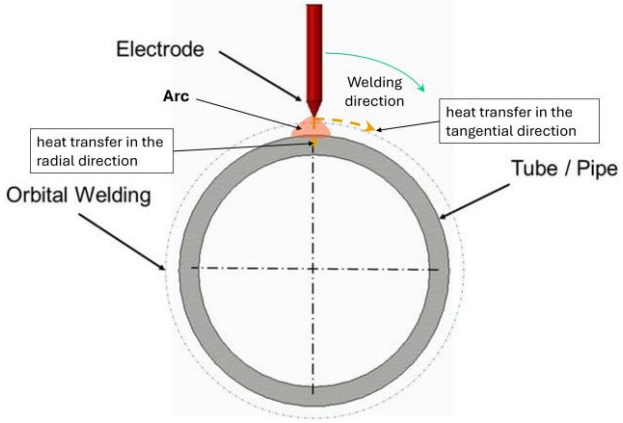

Fig. 5 The principle for thermal conductivity in Orbital TIG Welding.

Microstructure analysis

With the faster heat transfer in the radial direction, the HAZ (Heat-Affected Zone) of all welds on Ø60mm pipes is larger than that of the Ø48mm and Ø89mm pipes. Observations of the microstructures in **Table 4** reveal clear differences in HAZ size among samples within the same group. In particular, for the S7 sample group, which exhibited the highest UTS, the HAZ width decreased progressively from 9.4 mm (Ø48) to 9.1 mm (Ø60) and 6.2 mm (Ø89). This indicates that, at the same HI value, the larger the pipe diameter, the smaller the HAZ area.
The difference in HAZ between the pipes may be attributed to the heat transfer rate per unit area, or heat flux, which has the symbol (Q"). The heat flux can be determined by dividing the heat transfer rate by the area through which the heat is being transferred [25].

$$\dot{Q}'' = \frac{\dot{Q}}{A} \quad (3.)$$

Where: $\dot{Q}''$ is heat flux (kW/mm^2).
$\dot{Q}$ is the heat transfer rate (kW).
A is a cross-sectional area of heat transfer (mm^2).

From Equation (3.), it can be seen that as the pipe diameter increases, the heat flux decreases because the cross-sectional area of heat transfer increases. Therefore, under the same HI and welding conditions, the heat flux is significantly affected by the change in pipe diameter, which leads to variations in penetration depth and HAZ. However, this result does not apply to sample groups S1, S2, and S3, which were welded with a low HI level (below 200 J/mm). With such low HI or insufficient preheating, the cooling process occurs more rapidly. In this case, the cooling rate becomes the primary factor forming the microstructure of the weld and the HAZ [26]. Observing microstructure at the cross-section of the specimen with the highest tensile strength (**Fig. 6**), there are clear differences among the three regions: base metal (BM), heat-affected zone (HAZ), and weld metal (WM). The WM region exhibits the largest grain size because the cooling rate at the weld is the slowest. The grain structure coarseness is also dependent on the cooling rate during the welding process. The degree of cooling in this welding depends on the heat input and the working temperature [10, 33].

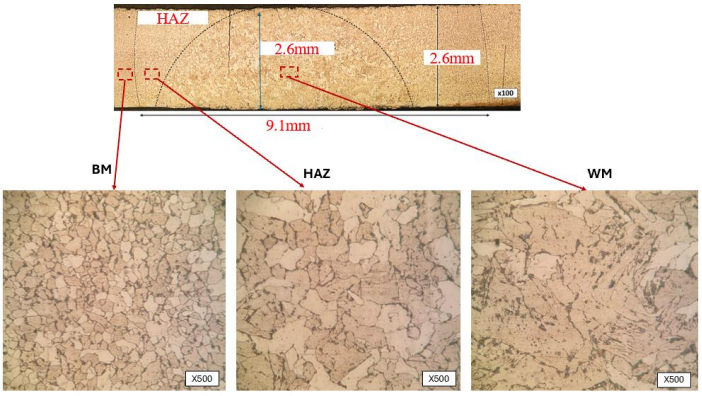

Fig. 6 Microstructure of the sample S7-60

Observations of the microstructures in the WM region of S7-48, S7-60, and S7-89 show that they all exhibit similarly coarse phase structures. These phases are primarily ferrite, as the welding temperature was insufficient to alter the structure of the base metal [10]. However, when measuring the average size of 10 random phases in the HAZ, it can be observed that the phase size of the S7-60 specimen is larger than that of the other specimens in the group. Although the same HI level of 390 J/mm was applied, differences in microstructures were found among specimens with varying diameters and thicknesses.

Table 5 Metallurgraphy of the S7 sample group at the X500 magnification

Sample	HAZ	WM
S7-48	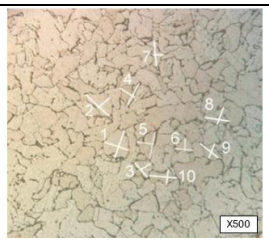 Length: 5.8µm; Width: 4µm	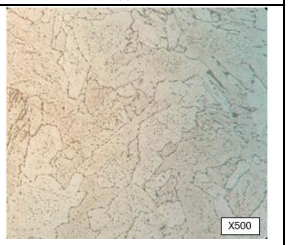
S7-60	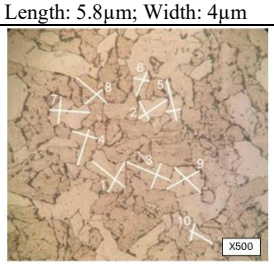 Length: 11.3µm; Width: 7.5µm	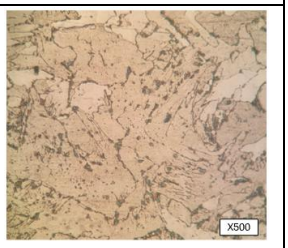
S7-89	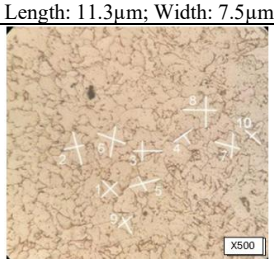 Length: 7.9µm; Width: 5.9µm	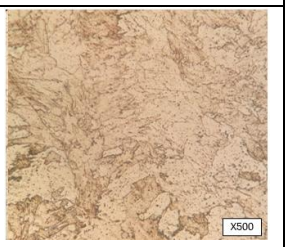

Taguchi and ANOVA analysis

The SN ratio analysis results from the Taguchi method **(Figs. 7, 8, 9)** represent an important step in evaluating and optimising the influence of HI-related factors on UTS.

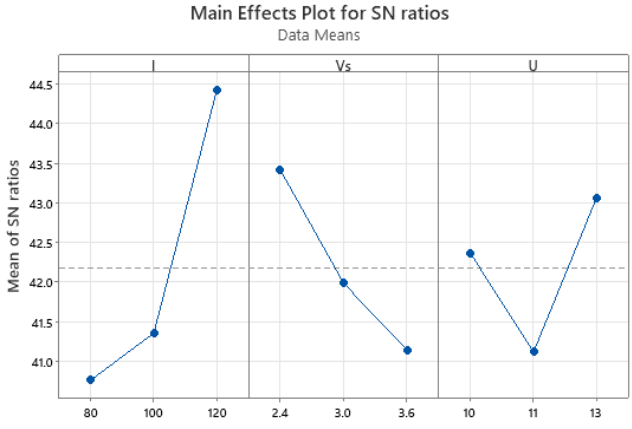

Fig. 7 Signal-to-noise: Larger is better for UTS of Ø48mm

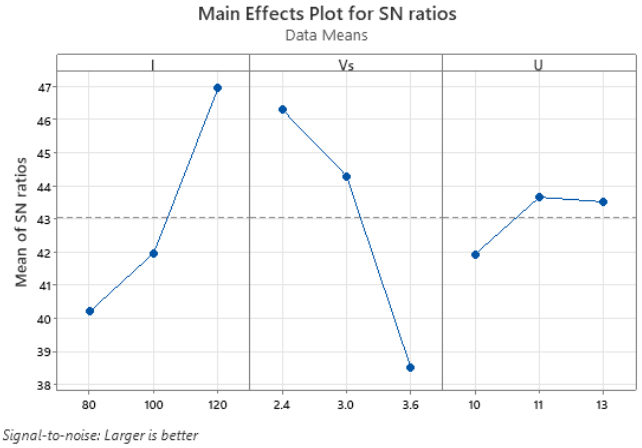

Fig. 8 Signal-to-noise: Larger is better for UTS of Ø60mm

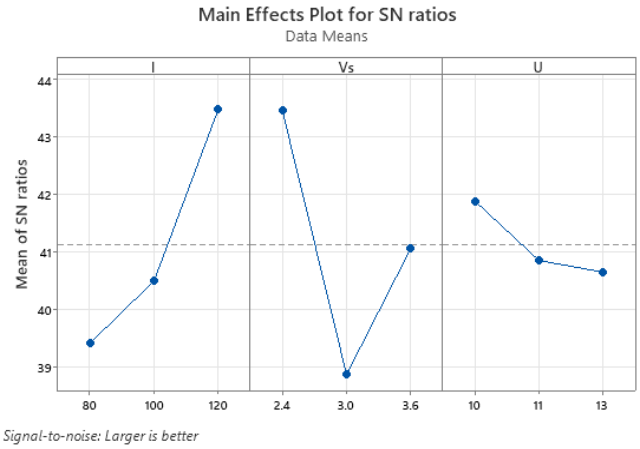

Fig. 9 Signal-to-noise: Larger is better for UTS of Ø89mm

Despite the differences in pipe diameters, among the three welding parameters investigated, welding current (I) and welding speed (Vs) still have the most significant impact on the UTS of the weld. These results are consistent with previous studies [12]. When the welding current (I) increases, the Heat Input (HI) also increases according to Equation (1.), resulting in a corresponding increase in UTS [10, 27]. On the other hand, increasing the welding speed (Vs) significantly reduces UTS due to the decrease in penetration [10, 27, 28]. Finally, although welding voltage (U) is also directly proportional to HI, increasing U by extending the arc length can lead to an unstable arc formation during the welding process.

The ANOVA analysis results show the ranking of the influence of welding parameters for each pipe size. For the Ø48x3.2mm pipe, the welding current has the most significant impact (**Table 6**) on UTS, with a contribution of 48.26% (**Table 7**), followed by the welding speed with 20.04%, and finally the welding voltage. These findings are consistent with those reported by Adigun et al. (2025) [29]. However, for the two pipes with larger diameters and thinner wall thicknesses, the ranking of influence on UTS changes. For the Ø60x2.6mm and Ø89x2.9mm pipes, the welding speed has the greatest impact, followed by welding current and finally welding voltage (**Table 6**). Referring to **Table 8**, the percentage contribution of welding current is still higher than that of welding speed, at 44.73% and 42.08%, respectively. However, this difference is not significant, as the F-values and P-values do not show large discrepancies, and the R^2 value of 88.42% obtained in this analysis is higher value than that reported by Abioye et al. [30]. This indicates a good correlation between the factors and UTS. As presented in **Table 9**, welding speed (Vs) has the greatest influence with a 51.12% contribution, while the contribution of welding current (I) is 46.65%. The lowest contribution is from voltage (U), with only 1.52%. This result confirms once again the significant influence of welding current and welding speed on UTS. It highlights that the relationship between welding current and welding

speed is fundamental to controlling HI and UTS, as also reported by Rohan Ishaan et al. [31]. Moreover, the F-value for Vs is higher than that of the other parameters, and the R^2 value of 99.30% in this analysis indicates an extremely strong correlation of this model.

Table 6 Response table for Signal to noise ratios for UTS of tubes.

Factor	I	Vs	U
Rank in Ø48mm	1	2	3
Rank in Ø60mm	2	1	3
Rank in Ø89mm	2	1	3

Table 7 Summary ANOVA for UTS of Ø48mm.

Source	DOF	SS	Contribution	MS	F-Value	P-Value
I	2	7201	48.26%	3600	3.05	0.247
Vs	2	2991	20.04%	1495	1.27	0.441
U	2	2367	15.86%	1183	1.00	0.500
Error	2	2363	15.84%	1181		
Total	8	14922	100.00%			
S = 34.3721; R^2 = 84.16%; R^2(adj) = 33.66%						

Table 8 Summary ANOVA for UTS of Ø60mm.

Source	DOF	SS	Contribution	MS	F-Value	P-Value
I	2	19698.0	44.73%	9849.0	3.86	0.206
Vs	2	18528.7	42.08%	9264.3	3.63	0.216
U	2	708.7	1.61%	354.3	0.14	0.878
Error	2	5100.7	11.58%	2550.3		
Total	8	44036.0	100.00%			
S = 50.8008; R^2 = 88.42%; R^2(adj) = 53.67%						

Table 9 Summary ANOVA for UTS of Ø89mm.

Source	DOF	SS	Contribution	MS	F-Value	P-Value
I	2	4677.6	46.65%	2338.78	66.61	0.015
Vs	2	5126.2	51.12%	2563.11	73.00	0.014
U	2	152.9	1.52%	76.44	2.18	0.315
Error	2	70.2	0.70%	35.11		
Total	8	10026.9	100.00%			
S = 5.92546; R^2 = 99.30%; R^2(adj) = 99.20%						

Based on the ANOVA analysis, the optimal welding parameter sets for each pipe size are proposed to achieve the highest UTS of the welds as follows:

Ø48x3.2mm: I= 120A, Vs = 2.4mm/s, U = 13V.

Ø60x2.6mm: I = 120A, Vs = 2.4mm/s, U = 11V.

Ø89x2.9mm: I = 120A, Vs = 2.4mm/s, U = 10V.

The predicted PJP weld behaviour in low-carbon tubes with diameters of Ø48, Ø60, and Ø89 was 218 MPa, 270 MPa, and 175 MPa, respectively. However, to achieve the required UTS for tubes or pipes welding used in high-pressure applications, further adjustment of welding parameters is necessary, particularly the welding current (I) and welding speed (Vs).

CONCLUSION

For the purpose of investigating the influence of different levels of Heat Input (HI) on pipe welds when the pipe dimensions vary, the research results showed that:

- With the same level of Heat Input (HI), the weld penetration and UTS of pipe welds vary noticeably when pipe dimensions change. However, changes in wall thickness should be given more attention than changes in.
- The Taguchi method indicates that welding current (I) and welding speed (Vs) have significant impacts on the UTS of the weld. In this case, for the smaller tube diameter of Ø48, the welding current (I) is the most influential factor, whereas for the larger diameters of Ø60 and Ø89, the welding speed (Vs) becomes the dominant factor.
- Based on the ANOVA analysis, the sets of parameters were predicted to produce PJP welds for each tube dimension, and the highest UTS was obtained with the Ø60×2.6 mm tube at 270 MPa.

Acknowledgements: This study is funded by Ho Chi Minh City University of Technology and Education (HCMUTE) for the project T2024-15.

REFERENCES

1. A. Calik, A. Duzgun, O. Sahin, N. Ucar: Zeitschrift für Naturforschung A, 65(5), 2010, 468-472. https://doi.org/10.1515/zna-2010-0512
2. S. Kou: *Welding metallurgy*, Wiley online books, 2002. https://doi.org/10.1002/0471434027
3. W.D. Callister: *Materials Science and Engineering: An Introduction*, New York: John Wiley & Sons, 7th Edition, 2006.
4. M.A. Bodude, I. Momohjimoh: Journal of Minerals and Materials Characterization and Engineering, 3(3), 2015, 142–153. https://doi.org/10.4236/jmmce.2015.33017
5. M. Panji, A.S. Baskoro, A. Widyianto: IOP Conference Series Materials Science and Engineering, 694(1), 2019, 012026. https://doi.org/10.1088/1757-899x/694/1/012026
6. R.W. Messler: *Principles of welding: processes, physics, chemistry and metallurgy*, New York: John Wiley & Sons, 2nd Edition, 2015.
7. R.H.G. De Silva, M.B. Schwedersky, Á.F. da Rosa: International Journal of Pressure Vessels and Piping, 188, 2020, 104229. https://doi.org/10.1016/j.ijpvp.2020.104229
8. G.L. de Oliveira, H.C. de Miranda, J.P. Farias: Welding International, 24(10), 2010, 749-757. https://doi.org/10.1080/09507110903568893
9. K.C. Riffel, R.H.G.E. Silva, G. Dalpiaz, C. Marques, M.B. Schwedersky: Soldagem & Inspeção, 24, 2019, e2418. https://doi.org/10.1590/0104-9224/si24.18
10. A.S. Baskoro, G. Kiswanto, A. Widyianto, M. Panji: International Journal of Integrated Engineering, 13(7), 2021, 288-296. https://doi.org/10.30880/ijie.2021.13.07.033
11. P. Joshi, P. Arunkumar: International Journal of Innovative Science, Engineering & Technology, 2(12), 2015, 958–959.
12. N.I.S. Hussein, M.N. Ayof, S. Nordin: International Journal of Materials Mechanics and Manufacturing, 4(1), 2015, 56–59. https://doi.org/10.7763/ijmmm.2016.v4.225
13. D.W. Figueirôa, I.O. Pigozzo, R.H.G.E. Silva, T.F. De Abreu Santos, S.L.U. Filho: Welding International, 31(8), 2017, 583–590. https://doi.org/10.1080/09507116.2016.1218615
14. G.V. Ngo: Materials Science Forum, 989, 2020, 766–771. https://doi.org/10.4028/www.scientific.net/msf.989.766
15. S. Shen, I.N.A. Oguocha, S. Yannacopoulos: Journal of Materials Processing Technology, 212(1), 2012, 286-294. https://doi.org/10.1016/j.jmatprotec.2011.09.013
16. R. Rai, S.M. Kelly, R.P. Martukanitz, T. DebRoy: Metallurgical and Materials Transactions A, 39, 2008, 98-112. https://doi.org/10.1007/s11661-007-9400-6
17. K.Y. Benyounis, A.G. Olabi, M.S.J. Hashmi: Journal of Materials Processing Technology, 164, 2005, 978-985. https://doi.org/10.1016/j.jmatprotec.2005.02.060
18. J. Nowacki, P. Rybicki: Journal of Materials Processing Technology, 164, 2005, 1082-1088. https://doi.org/10.1016/j.jmatprotec.2005.02.079
19. ASTM International: *A53/A53M – 12 Standard specification for pipe, steel, Black and Hot-Dipped, Zinc-Coated, Welded and seamless*: 2012.
20. H. E. Lakache, A. May, R. Badji: Acta Metallurgica Slovaca, 29(3), 2023, 155-160. https://doi.org/10.36547/ams.29.3.1883
21. The American Society of Mechanical Engineers: An International Code 2019 ASME Boiler & Pressure Vesel Code, Section IX: *Welding, Brazing and Fusing Qualifications* (ASME BPVC.IX-2019): 2019.
22. International Standard: *Metallic materials - Tensile testing - Part 1: Method of test at room temperature*, Third edition. ISO 6892-1: 2019.

23. T.T. Nguyen, V.H. Hoang, V.T. Nguyen, V.T.T. Nguyen: Journal of Manufacturing and Materials Processing, 8(5), 2024, 219. https://doi.org/10.3390/jmmp8050219
24. Y.K. Khdir, S.A. Kako, R.H. Gardi: Polytechnic Journal, 10(1), 2020, 1-5. https://doi.org/10.25156/ptj.v10n1y2020.pp1-5
25. U. S. D. O. Energy: *DOE Fundamentals Handbook - Thermodynamics*, Heat Transfer, and Fluid Flow (Volume 2 of 3): 2016.
26. R.S. Funderburk: *A Look at Input, Key Concepts in Welding Engineering*, Welding Innovation,Vol. XVI, No. 1, 1999.
27. Ľ. Kaščák, J. Slota, J. Bidulská, R. Bidulsky, A. Kubit: Acta Metallurgica Slovaca, 29(4), 2023, 214–218. https://doi.org/10.36547/ams.29.4.1979
28. E. Fracchia, J. Bidulská, R. Bidulský, M. Actis Grande: Materials, 15(2), 2022, 412. https://doi.org/10.3390/ma15020412
29. O. Adigun, A. Adebayo, O. Abiola: American Journal of Mechanical and Materials Engineering, 9(1), 2025, 37-42. https://doi.org/10.11648/j.ajmme.20250901.14
30. T. Abioye, C. Kanu, T. Ogedengbe, D. Adebiyi: International Journal of Microstructure and Materials Properties, 14(2), 2019, 155-169. https://doi.org/10.1504/ijmmp.2019.099225
31. J. Mucha, L. Kaščák, E. Spišák: Civil and Mechanical Engineering, 11, 2011, 135-148. https://doi.org/10.1016/S1644-9665(12)60179-4
32. J. Mucha, L. Kaščák, E. Spišák: Advances in Mechanical Engineering, 2013, 2013, 848973. https://doi.org/10.1155/2013/848973
33. I.S. Asibeluo, E. Emifoniye: International Journal of Mechanical Engineering, 2(9), 2015, 32–40. https://doi.org/10.14445/23488360/ijme-v2i9p113